Mesomorphic Properties of a Metallomesogen Based on a Copper(II) Metal-Chain Structure

Lee Y. Park* and James M. Rowe

Department of Chemistry, Williams College, Williamstown, Massachusetts 01267

Received December 10, 1997. Revised Manuscript Received February 6, 1998

Liquid crystalline properties have been introduced into one-dimensional metal-chain complexes based on Cu(pyridine)$_2$X$_2$ via straightforward derivatization of the pyridyl ligands. When the aliphatic portion of the mesogen is introduced via an ester, no mesophase behavior is observed; however, when an amide group is used as the means of incorporating the flexible portion of the molecule, a mesogenic material results. The structure of these amide-derivatized materials is different when obtained from solution vs from the melt, due to changes in the hydrogen-bonding framework formed along the chain. The solution-derived material does not display any mesophase behavior, whereas the material derived from the melt does. The thermal behavior of these materials is somewhat complicated by the variety of noncovalent interactions (hydrogen bonds, metal−halide bridging interactions) involved. By including hydrogen-bonding groups in the ligands at positions opposite to the metal-coordination site it is possible to significantly affect the environment of the metals in these complexes, presumably via compression of the bridging Cu−X bonds.

Introduction

One of the primary difficulties associated with developing one-dimensional magnetic, optical, or electrical materials is that maximum anisotropy requires "perfect" domains; practical applications are therefore limited by the ease with which single crystals of a given material can be grown.[1−3] The incorporation of the physical properties of liquid crystals into such one-dimensional materials is an attractive solution to this problem. It is easy to imagine that defects in a one-dimensional structure could be repaired by annealing a liquid crystalline material in the fluid phase, followed by quenching, thereby achieving relatively large-scale domains. With these types of goals in mind, the area of metal-containing liquid crystals has been quite active in recent years,[4] and examples of metallomesogens with high magnetic anisotropy,[5] ferroelectric behavior,[6] and potential as optical storage devices[7] have been reported. A general strategy employed in designing many new metallomesogens is to prepare discrete metal complexes with ligands that impart the requisite molecular geometry to the complex (generally rodlike or disklike), relying on the intermolecular interactions ($\pi-\pi$ stacking of ligands, dipole−dipole interactions) and the overall molecular geometry of the complex to induce the molecular alignment in the liquid crystalline phase.[8−10] A number of more complex molecular shapes giving rise to mesophases have also been developed using a similar approach.[11−13] The objective of the work described here was to investigate whether the design of metallomesogens could be approached from a slightly different perspective. Rather than forming discrete metallomesogens whose alignment in the fluid phase relies on the aggregation of individual molecules, we were interested in inducing mesophase behavior in known metal-chain complexes.

Our initial studies have focused on the well-known chain structures found in *trans*-Cu(pyridine)$_2$X$_2$, which have been extensively studied as models for one-dimensional magnetic behavior.[14,15] In these complexes, halides on one square planar unit bridge to the open coordination sites on adjacent centers, forming −M(pyridine)$_2$(μ-X)$_2$− chains, a coordination polymer with pseudo-octahedral (elongated tetragonal) coordination around each metal center, as shown in Figure 1.[16−18]

(1) Miller, J. S.; Epstein, A. J. In *Progress in Inorganic Chemistry*; Lippard, S. J., Ed.; Wiley: New York, 1975; Vol. 20.
(2) *Synthesis and Properties of Low-Dimensional Materials*; Miller, J. S., Epstein, A. J., Eds.; New York Academy of Sciences: New York, 1977; Vol. 313.
(3) *Extended Linear Chain Compounds*; Miller, J. S., Ed.; Plenum: New York, 1982.
(4) *Metallomesogens*; Serrano, J. L., Ed.; VCH: Weinheim, 1996.
(5) Galyametdinov, Y.; Athanassopoulou, M. A.; Griesar, K.; Kharitonova, O.; Soto Bustamante, E. A.; Tinchurina, L.; Ovchinnikov, I.; Haase, W. *Chem. Mater.* **1996**, *8*, 922.
(6) Iglesias, R.; Marcos, M.; Serrano, J. L.; Sierra, T.; Perez-Jubindo, M. A. *Chem. Mater.* **1996**, *8*, 2611.
(7) Buey, J.; Diez, L.; Espinet, P.; Kitzerow, H. S.; Miguel, J. *Chem. Mater.* **1996**, *8*, 2375.
(8) Maitlis, P. M.; Bruce, D. W.; Dhillon, R.; Dunmur, D. A.; Fanizzi, F. P.; Hunt, S. E.; Le Lagadec, R.; Lalinde, E.; Orr, R.; Rourke, J. P.; Salt, N. J. S.; Stacey, J. P.; Styring, P. *New J. Chem.* **1990**, *14*, 549.
(9) Espinet, P.; Esteruelas, M. A.; Oro, L. A.; Serrano, J. L.; Sola, E. *Coord. Chem. Rev.* **1992**, *117*, 215.
(10) Giroud-Godquin, A.-M.; Maitlis, P. M. *Angew. Chem., Int. Ed. Engl.* **1991**, *30*, 375.
(11) Zheng, H.; Swager, T. M. *J. Am. Chem. Soc.* **1994**, *116*, 761.
(12) Serrette, A. G.; Swager, T. M. *J. Am. Chem. Soc.* **1993**, *115*, 8879.
(13) Baena, M. J.; Barbera, J.; Espinet, P.; Ezcurra, A.; Ros, M. B.; Serrano, J. L. *J. Am. Chem. Soc.* **1994**, *116*, 1899.
(14) Jeter, D. Y.; Hatfield, W. E. *J. Inorg. Nucl. Chem.* **1972**, *34*, 3055.
(15) Takeda, K.; Matsukawa, S.; Haseda, T. *J. Phys. Soc. Jpn.* **1971**, *30*, 1330.
(16) Morosin, B. *Acta Crystallogr.* **1957**, *B31*, 632.
(17) Estes, W. E.; Gavel, D. P.; Hatfield, W. E.; Hodgson, D. J. *Inorg. Chem.* **1978**, *17*, 1415.

S0897-4756(97)00799-0 CCC: $15.00
Published on Web 03/18/1998

Chart 1

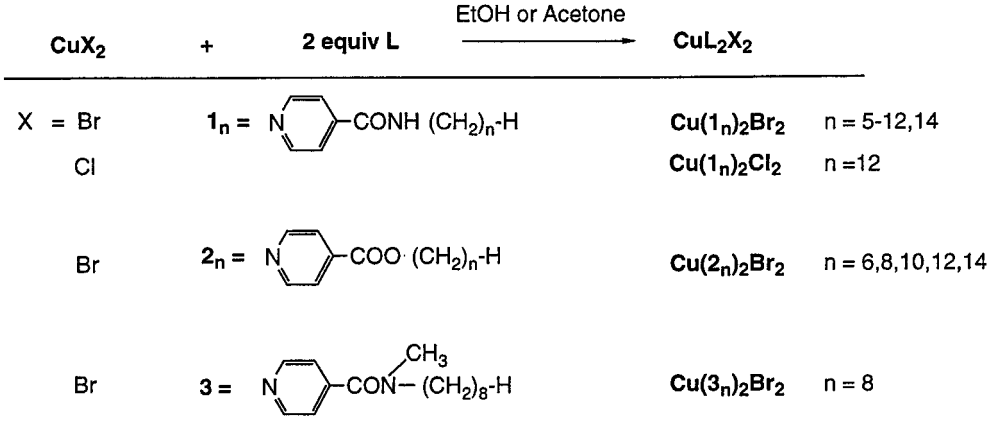

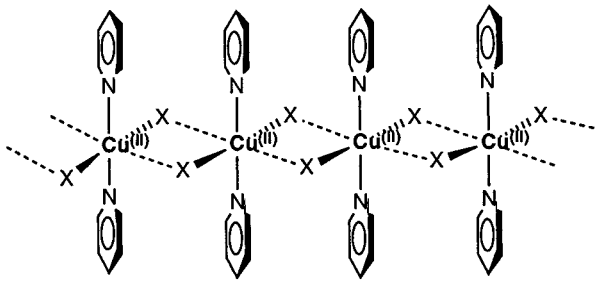

Figure 1. Extended chain structure formed by bridging halide interactions in Cu(pyridine)$_2$X$_2$.

The first goal was to introduce mesogenic properties into these chainlike structures by incorporating a long aliphatic chain into the monomeric M(pyridine)$_2$X$_2$ units. The expected mesophase of this type of structure would best be described as "ribbonlike". There are examples of organic liquid crystalline materials that are structurally analogous to this system,[19,20] as well as a number of polymeric structures whose backbones are constructed from monomers which aggregate via noncovalent interactions.[21]

The second goal of this work was to investigate the influence of interligand hydrogen bonding on the backbone of the structure. It is well understood that the stability of a mesophase may be tuned through careful control of intermolecular interactions in the form of hydrogen-bonding and dipole−dipole interactions.[22−24] In studies of solid-state one-dimensional metal-chain systems it has been shown that these types of intermolecular interactions can distort the dimensions along the metal chains, leading to materials with improved one-dimensional properties.[25−27] We were interested in trying to combine these effects to see whether incorporation of hydrogen-bonding functionalities into our ligands can provide attractive forces between adjacent metal units in order to both stabilize mesophase behavior as well as to affect the bridging M−X bonds, possibly leading to higher intrachain magnetic coupling than in the parent structures. Though the magnetic behavior of these materials has not yet been investigated, we are able to demonstrate that hydrogen bonding between adjacent monomers units does have a significant impact on both the thermal behavior of these materials, resulting in a stabilized mesophase, as well as on the chain structure of our materials, resulting in a measurable change in the electronic environment at the metal center.

Results and Discussion

The complexes indicated in Chart 1 were prepared by addition of a stoichiometric amount of the appropriate isonicotinoate esters or amides to a solution of CuX_2 in either ethanol or acetone;[14,28] the bromide complexes precipitated as soft bright green solids (the chlorides gave blue solids) and were isolated by filtration to give analytically pure materials. Our studies focused primarily on the amide series, **Cu(1$_n$)$_2$X$_2$**, which showed the most promising mesogenic behavior. Within this family, the bromides were of greater interest than the chlorides due to their enhanced thermal stability and the larger magnetic coupling that has been observed between copper atoms in the parent Cu(pyridine)$_2$X$_2$ complexes.[17,29]

The amide complexes exhibit interesting thermal behavior: as prepared from solution, the materials exhibit no liquid crystalline phase upon heating. However, after the initial isotropization, a liquid crystalline phase is observed on cooling as well as on all subsequent heatings; that is, the material prepared from the melt does exhibit liquid crystalline behavior. In contrast, neither the monoester complexes, **Cu(2$_n$)$_2$X$_2$**, nor the *N*-methyl octyl complex, **Cu(3$_8$)$_2$X$_2$**, exhibit this type of behavior, suggesting that hydrogen-bonding interactions between ligands on adjacent metal centers are responsible for the thermal behavior observed.

Mesomorphism of Cu(1$_n$)$_2$X$_2$ Complexes. By polarized optical microscopy, all members of this series of

(18) Marsh, W. E.; Valente, E. J.; Hodgson, D. J. *Inorg. Chim. Acta* **1981**, *51*, 49.
(19) Matsunaga, Y.; Terada, M. *Mol. Cryst. Liq. Cryst.* **1986**, *141*, 321.
(20) Malthête, J.; Levelut, A.-M.; Liebert, L. *Adv. Mater.* **1992**, *4*, 37.
(21) Paleos, C. M.; Tsiourvas, D. *Angew. Chem., Int. Ed. Engl.* **1995**, *34*, 1711.
(22) Leadbetter, A. J. *Thermotropic Liquid Crystals*; Wiley: New York, 1987; Vol. 22.
(23) Kelker, H.; Hatz, R. *Handbook of Liquid Crystals*; Verlag Chemie: Weinheim, 1980.
(24) Toyne, K. J. *Thermotropic Liquid Crystals*; Wiley: New York, 1987; Vol. 22.
(25) Okamoto, H.; Toriumi, K.; Okaniwa, K.; Mitani, T. *Synth. Met.* **1991**, *41−43*, 2791.
(26) Bekaroglu, O.; Breer, H.; Endres, H.; Keller, H. J.; Nam Gung, H. *Inorg. Chim. Acta* **1977**, *21*, 183.
(27) Clark, R. J. H. *Chem. Soc. Rev.* **1990**, *19*, 107.
(28) Gill, N. S.; Nyholm, R. S. *J. Inorg. Nucl. Chem.* **1961**, *18*, 88.
(29) Crawford, V. H.; Hatfield, W. E. *Inorg. Chem.* **1977**, *16*, 1336.

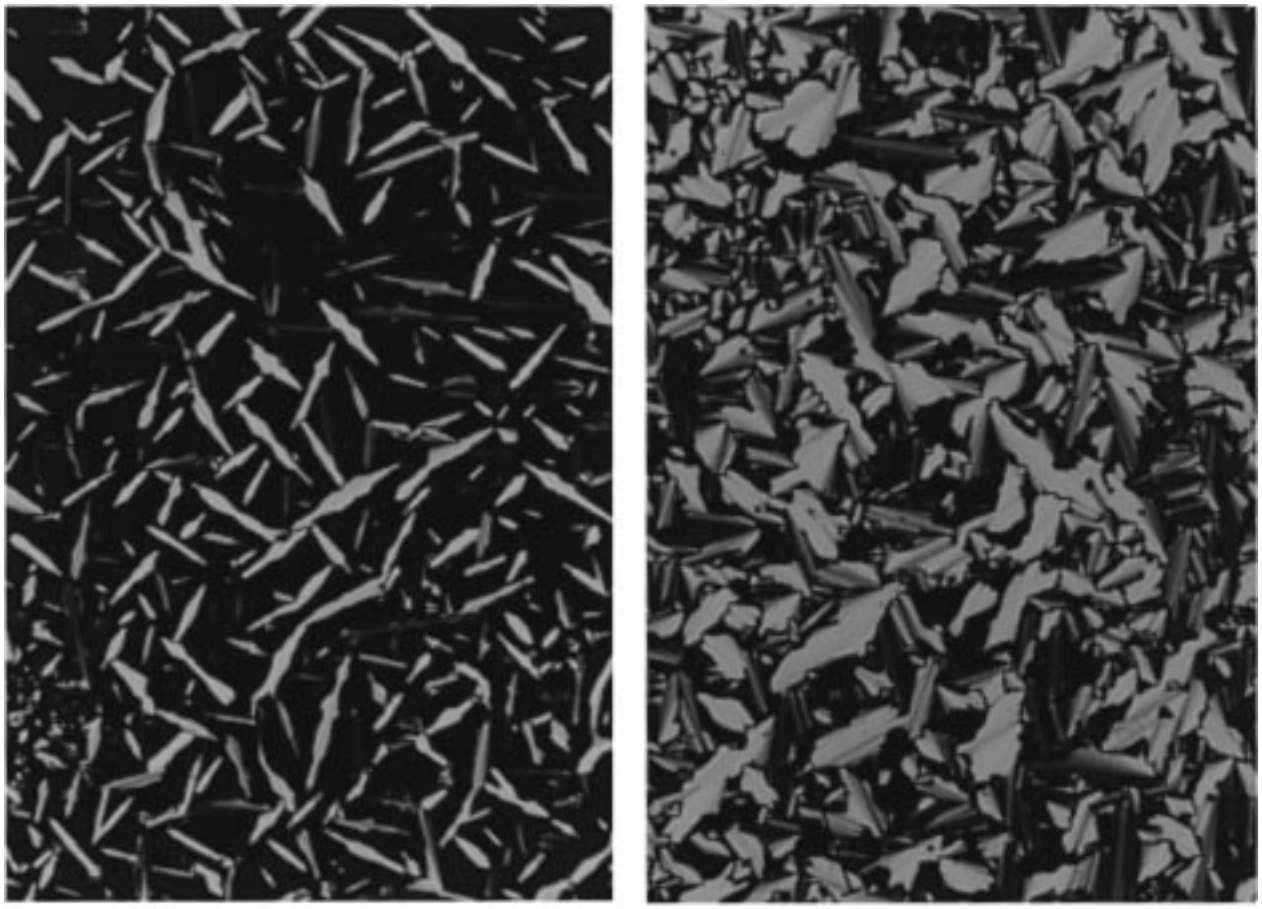

Figure 2. (a) Bâtonnet texture of $\mathbf{Cu(1_{10})_2Br_2}$. (b) Evolution of focal conic texture of $\mathbf{Cu(1_{10})_2Br_2}$ from bâtonnet texture (10× magnification).

complexes exhibit similar behavior: the first visible change (on first heating) occurs when the solid melts to a fluid birefringent phase (at ~210 °C), which then quickly clears to give an isotropic liquid. There is no variation in melting point with length of the aliphatic chain. Upon cooling, a very fluid mesophase develops. This mesophase is characterized by an optical texture in the form of bâtonnets (Figure 2a), which grow in to give a focal conic texture (Figure 2b), indicative of a layered mesophase.

On the second heating, the behavior is quite different than the first, though identical to all subsequent heatings; there is no difference between the first and any subsequent coolings. The material becomes fluid well below the clearing point, which in this case occurs at a significantly lower temperature than on the first heating; temperatures for these transitions vary with the length of the aliphatic chain. The initial high-temperature melting and reordering above 200 °C never reoccurs. This behavior initially suggested some type of decomposition; however, under the protection of a microscope cover slip, the complexes appear to be relatively stable at these temperatures. Elemental analyses before and after melting do not indicate any change in elemental composition; in addition, the brownish-green material produced upon melting can be converted back to the original green material upon redissolution in ethanol. Nor is there any evidence via electron spin resonance (ESR), far-IR, magnetic susceptibility measurements, or by analysis of the phase behavior of the ligands alone to suggest that phase separation of the ligands from the metal is occurring. Finally, ESR studies along with X-ray and differential scanning calorimetry (DSC) data (discussed below) suggest that the overall molecular architecture of the material remains intact after this first high-temperature melting.

Neither the ester complexes, $\mathbf{Cu(2_{\mathit{n}})_2X_2}$, nor the *N*-methyl amide complex, $\mathbf{Cu(3_8)_2X_2}$, exhibit this type of first melting behavior; these melt cleanly to isotropic liquids (at around 175 and 155 °C, respectively), with no change in color, and their thermal behavior does not vary with subsequent heatings. The much higher initial melting point observed for the amide complexes indicates that the behavior observed must be due to hydrogen-bonding interactions. In $\mathbf{Cu(1_{\mathit{n}})_2X_2}$, lability of the pyridyl ligands at the high temperatures needed to achieve the first melting (thermal decomposition via loss of pyridine in the parent $Cu(pyridine)_2Br_2$ begins at approximately 190 °C) allows the overall structure to reorient to give the lower melting material.

DSC traces for one member of the amide series, $\mathbf{Cu(1_{14})_2Br_2}$, are illustrated in Figure 3. A number of the transitions observed by DSC are broad and their positions are highly dependent on the thermal history of the sample. This is not surprising given the variety of noncovalent interactions involved in forming the chain-like structure.[30,31] The initial heating scan of **Cu-**

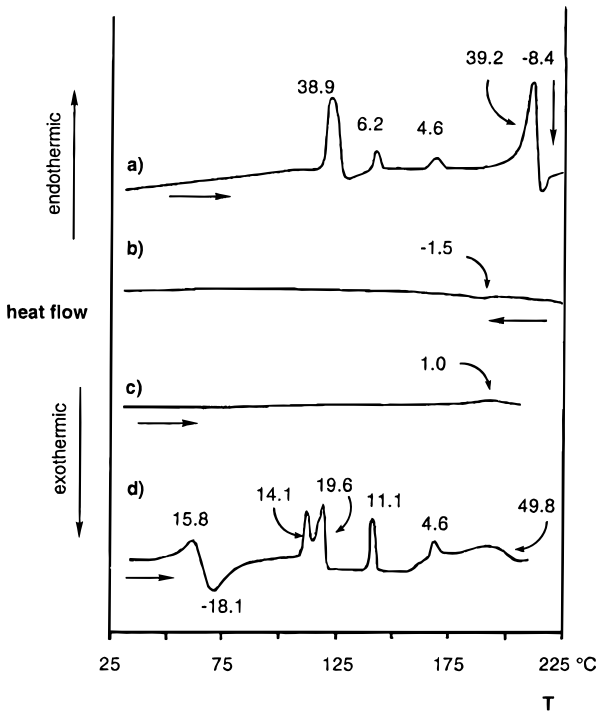

Figure 3. DSC traces of $\mathbf{Cu(1_{14})_2Br_2}$ (a) on first heating, (b) on first cooling, (c) on second heating (immediately after first cooling), and (d) on second heating (after annealing at room temperature for 3 weeks following the first heating and cooling). Enthalpies for each transition are indicated above each peak in kJ/mol.

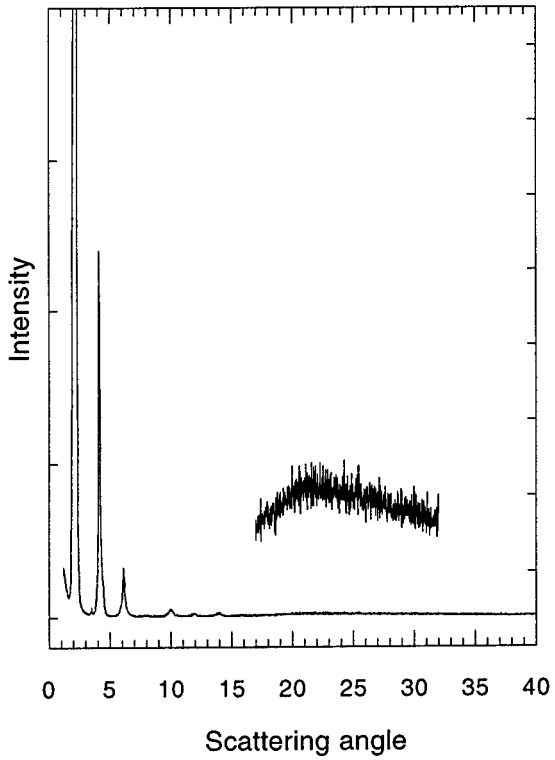

Figure 4. Room temperature X-ray diffraction spectrum of $\mathbf{Cu(1_{12})_2Br_2}$ after annealing in mesophase and quenching.

$\mathbf{(1_{14})_2Br_2}$ is shown in Figure 3a. The most distinctive feature is a large endotherm around 210 °C followed immediately by a smaller exotherm at 216 °C, corresponding to the melting and reordering observed via microscopy; there is no distinct endotherm corresponding to the clearing, suggesting that the reordered material is not stable at this temperature, as described above. On cooling typically only a single very small transition is observed at 185 °C (Figure 3b), indicating a strong tendency toward supercooling; this single small exothermic peak corresponds to the temperature at which the bâtonnet texture appears on the polarizing microscope. Even at relatively slow scan rates (1 °C/min) we are not able to see any other exothermic transitions when cooling from the isotropic melt. An immediate second heating scan (Figure 3c) reveals little, as would be expected. However, when a sample is allowed to anneal at room temperature (after the initial isotropization) for 2−3 weeks, a second heating scan reveals the series of endotherms as shown in Figure 3d. The transitions observed on this second heating match the initial heating scan relatively well (with the exception of the first isotropization), and there is no significant loss in enthalpies; these results are consistent with the belief that the solution structure is different from the melt structure, but that the overall molecular connectivity remains intact.

Each of the observed transitions (around 110, 140, and 170 °C) is reversible; the corresponding exothermic peaks may be observed on cooling provided that the cooling scan begins before isotropization, which is associated with the very broad transition that appears between 165 and 200 °C. The transition at 110 °C is most likely due to a melting of the alkyl chains; the corresponding recrystallization exhibits a strong tendency toward supercooling and often appears more than 50 °C lower than the melting (the free ligands show similar thermal behavior.) As the material does not always reorder completely upon cooling, an exotherm is often observed on the next heating scan, as shown in Figure 3d. Above 110 °C the sample can be sheared only with difficulty, and very slight changes in the optical texture may be observed; however, the phase is extremely viscous, and variable temperature X-ray diffraction of the sample just above 110 °C (on samples that have been thermally treated[32]) indicates that the material still possesses crystalline order.

The transition at 140 °C leads to a true fluid mesophase. X-ray data were obtained by annealing the sample on a microscope slide above 140 °C (after an initial isotropization), quenching on dry ice, followed by immediate collection of the diffraction pattern at room temperature (see Figure 4). Data obtained in this manner show clear evidence of a layered mesophase (S_A-like), as expected based on the observed optical textures and the structure of our materials, with diffraction peaks at angles (2.1° and harmonics) corresponding to a fully extended molecular length (42 Å) and with a

(30) Lee, C.-M.; Griffin, A. C. *Macromol. Symp.* **1997**, *117*, 281.
(31) Lillya, C. P.; Baker, R. J.; Hutte, S.; Winter, H. H.; Lin, Y. G.; Shi, J.; Dickinson, L. C.; Chien, J. C. W. *Macromolecules* **1992**, *25*, 2076.

(32) If this phase is studied upon cooling from a higher temperature phase, it appears to be liquid crystalline. Therefore, it was necessary to prepare the sample by heating to the isotropic phase followed by cooling and annealing at room temperature for two to three weeks before collecting X-ray diffraction data upon heating. Under these conditions, the sample is clearly crystalline in this temperature range (between 110 and 140 °C.)

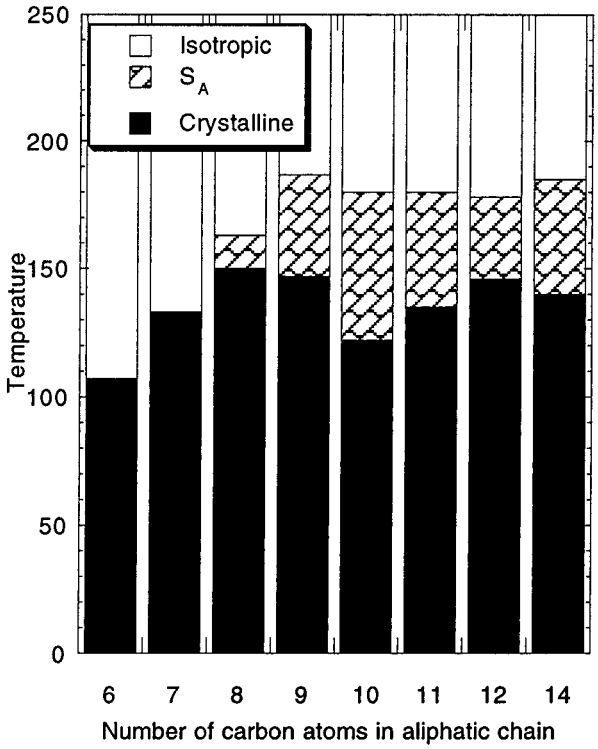

Figure 5. Phase diagram for $\mathbf{Cu(1_n)_2Br_2}$ series. All transition temperatures are taken from second (or subsequent) DSC heating runs except for the isotropization temperatures which were taken from microscopy studies. Because the molecular weight of the samples is expected to vary from run to run, as a function of thermal history, temperatures must be taken as approximate.

diffuse halo at wide angles (Figure 4 inset.) Analogous results were obtained for the other members of the series. Interestingly, when we tried to collect "in-phase" X-ray data at high temperature (in packed capillary tubes), our results were less clear. The diffraction patterns obtained in these cases indicated only extremely weak diffraction and did not correspond well to either the quenched X-ray experiments or to the expected structures of our materials. The difficulty in obtaining satisfactory in-phase X-ray data may be due to the fact that the observed mesophase is metastable (since the original crystalline phase is higher melting than the observed mesophase), and that by quenching the mesophase we are able to freeze the structure in and thereby observe its X-ray pattern. Upon trying to obtain the diffraction pattern at high temperature, we are only able to approach the temperature fairly gradually, so that the diffraction pattern observed at high temperature may correspond to some other thermodynamically more stable structure. Another possibility is that the sample is not sufficiently stable upon exposure to X-ray radiation at high temperatures for the long periods of time required to collect the diffraction data.

This mesophase is observed for all members off the series where $n > 8$ (see Figure 5). It is surprising that these materials would give rise to the very fluid mesophase observed, given such a low density of aliphatic chains on a rigid backbone. It is likely, therefore, that the bridging halide interactions (which would impose rigidity on the backbone) are not intact in the mesophase; this is reasonable considering the temperature range of the mesophase. Instead, the hydrogen-bonding framework is most likely responsible for maintaining a flexible "ribbonlike" structure, which is consistent with the fact that the non-hydrogen bond forming ligands do not give rise to mesomorphic complexes. In addition, we have prepared examples of analogous complexes containing 3,5-pyridine diesters and have found that by increasing the aliphatic chain density (thereby lowering the temperature range of the mesophase) the hydrogen-bonding framework is no longer needed to stabilize the mesophase.

It was not possible to determine the nature of the material past the transition at 170 °C since it is superimposed on the very broad peak associated with isotropization. The exact position and breadth of this broad feature varies widely from sample to sample and with thermal history. We assume that this peak corresponds to disruption of the various noncovalent interactions holding the chain structure together—the hydrogen bonding between adjacent monomer units, as well as the coordination of the pyridines to the metals.

Effect of Intermolecular Hydrogen Bonding in $\mathbf{Cu(1_n)_2X_2}$ Complexes. The data presented in the previous section establish that the presence of hydrogen-bonding functionalities in these systems plays a critical role in stabilizing the mesophase behavior of the chain structures. A number of other effects related to these same hydrogen-bonding interactions may also be observed. For instance, all of the amide complexes, $\mathbf{Cu(1_n)_2X_2}$, undergo a significant color change upon melting, from green to greenish-brown in the case of the bromides and from blue to green in the case of the chlorides. The original green and blue solids can be regenerated by dissolving the melted and cooled samples in ethanol. In contrast, neither the analogous ester complexes [$\mathbf{Cu(2_n)_2X_2}$] nor the *N*-methyloctyl amide complex [$\mathbf{Cu(3_8)_2X_2}$] exhibit a color change upon melting.

ESR spectra of the parent complexes have been previously studied and have shown that the Cu(II) environment is measurably different in $Cu(pyridine)_2Br_2$ than in $Cu(pyridine)_2Cl_2$,[17,29] though both possess the chain structure shown in Figure 1, as demonstrated via crystallography.[16] A clear tetragonal environment is observed for the Cu^{2+} in the chloride complex, whereas a single very broad resonance is observed for the bromide; these results are consistent with the greater magnetic exchange interaction observed for the bromide species. ESR spectra of our complexes are intriguing. For the $\mathbf{Cu(1_n)_2X_2}$ series of complexes, as prepared from solution, ESR spectra are consistent with a tetragonal Cu(II), as shown in Figure 6a for $\mathbf{Cu(1_{14})_2X_2}$. In contrast, only a single very broad resonance is observed for the ester complexes ($\mathbf{Cu(2_n)_2X_2}$), suggesting that the tetragonal elongation is more pronounced in the amide complexes than in the ester complexes. After thermal treatment (melting to the isotropic phase, followed by annealing in the mesophase, and cooling to room temperature), however, the ESR spectra of the amides change to give the single very broad signal shown in Figure 6b, much like the broad resonance observed for the parent $Cu(pyridine)_2Br_2$, while the ESR spectra of the esters are unchanged by similar thermal treatment. This suggests that the tetragonal distortion of the Cu^{2+} environment has become significantly less pronounced,

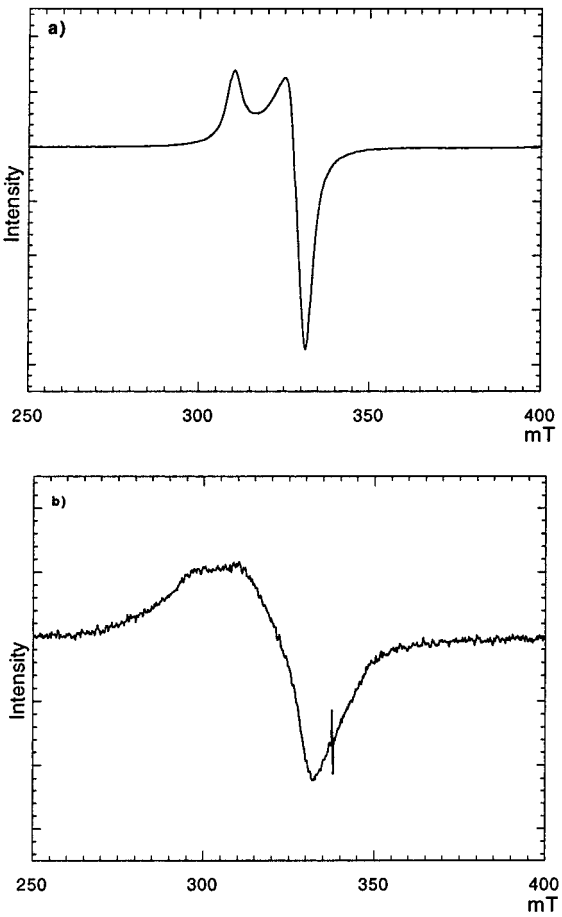

Figure 6. (a) ESR spectrum of $\mathbf{Cu(1_{14})_2Br_2}$ as prepared from solution. (b) ESR spectrum of $\mathbf{Cu(1_{14})_2Br_2}$ after melting to isotropic followed by slow cooling (the spike at 340 mT is an instrumental artifact). The vertical scales for the two spectra are identical.

due to the effect of hydrogen bonding between adjacent ligands during the reordering of these materials as they cool from the melt. The same behavior is observed for both the chlorides and the bromides in this series. As further confirmation, a tetragonal Cu^{2+} environment (presumably due to steric interactions) is observed in the ESR spectra of the *N*-methyloctyl amide complex $\mathbf{Cu(3_8)_2Br_2}$ with no change upon melting.

IR spectra of $\mathbf{Cu(1_n)_2X_2}$ are also consistent with these observations. A relatively sharp signal is seen for the NH stretch at 3320 cm^{-1} in the material isolated from solution. After the thermal treatment similar to that described above, this signal is largely diminished, and is replaced by a broader signal that is shifted to higher wavenumbers. A slight broadening of the CO stretch is also observed.

The most reasonable explanation for the difference between the solution vs melt structures involves the relative orientation of the pyridyl ligands on adjacent metals. If the ligands on adjacent metals are oriented in an approximately edge-to-edge orientation (in which the plane of the pyridine ligands is approximately in the same plane as the metal-chain axis), strong hydrogen-bonding interactions can form between the carbonyl on one ligand and the amide proton on the adjacent ligand (see Figure 7a). This orientation would result in a relatively large Cu−Br bridging distance and would account for the tetragonal distortion indicated by the

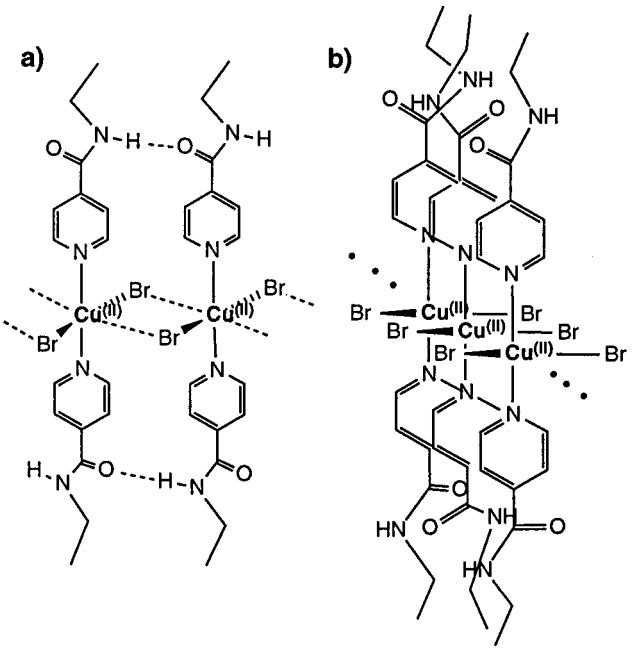

Figure 7. (a) Proposed structure of $\mathbf{Cu(1_n)_2Br_2}$ as formed from solution (plane of pyridine rings and chain axis in plane of page). (b) Proposed structure of $\mathbf{Cu(1_n)_2Br_2}$ as formed from melt (plane of chain axis perpendicular to plane of pyridine rings and plane of page).

ESR data. Upon melting, this hydrogen bonding is disrupted and the pyridine ligands become labile, allowing them to reorient in an approximately face-to-face orientation (see Figure 7b) in which the plane of the pyridine ligands is no longer aligned with the metal-chain axis. This type of orientation would allow for closer approach of adjacent metal centers, thus shortening the Cu−Br bridging bonds, and would account for the change observed in the ESR spectra. The hydrogen bonding in this type of arrangement would be much less directed and therefore considerably weaker than in the solution structure, consistent with the stronger NH stretch observed in the IR after initial melting, and would explain the lowered clearing point observed upon second melting. In the face-to-face orientation, the aliphatic chains are packed much more densely than in the edge-to-edge orientation, which may partially account for the ability of the face-to-face oriented material to support a mesophase. (The structures indicated in Figure 7 are intended to illustrate extreme cases of the two orientations described.) The high fluidity of the mesophase and the absence of evidence in the X-ray data pointing to interchain order lead us to believe that *inter*chain hydrogen bonding does not play a significant role in the behavior observed.

Conclusions

Two important goals have been achieved in this work. First, we have been able to introduce liquid crystalline behavior into a one-dimensional metal-chain structure, giving rise to a lamellar mesophase, as expected. Hydrogen bonding between adjacent metal units is critical in stabilizing the mesophase in our compounds, giving rise to a layered mesophase that may be analogous to the "ribbonlike" mesophases that have been described in some organic systems.[20,21] Second, we have

seen preliminary indications that the metal−metal interactions along the metal-chain structure can be significantly affected by interactions between ligands even when they are not within the immediate coordination sphere of the metals. In future work, we will continue our studies on these and related metal-chain systems, and will begin a detailed study of their magnetic exchange properties.

Experimental Section

General Methods. NMR spectra were run on a Bruker Avance DPX300 in $CDCl_3$ (unless otherwise specified) and referenced to residual $CHCl_3$. ESR spectra were run on a JEOL RE1X. Magnetic susceptibility measurements were made on a Johnson-Matthey balance. Optical Microscopy was carried out using standard covered glass microscope slides on an Olympus BX50 polarizing microscope using an Instec HS400 heating stage with an RTC1 temperature controller. DSC and TGA analyses were performed on Perkin-Elmer Series 7 instruments in conjunction with a Perkin-Elmer 7700 Thermal Analysis Data Station. Room temperature X-ray data were carried out on a Phillips XRG 3100. Variable temperature X-ray measurements were taken on an Inel CPS120 position sensitive detector using an XRG 2000 generator (Cu Kα), and the temperature was controlled using a Minco CT137 controller; solid samples were packed into 1.5 mm glass capillary tubes and sealed. Satisfactory elemental analyses were obtained for all of the copper complexes studied; elemental analyses were performed either by the University of Michigan (Ann Arbor) in-house analytical services or by Midwest Microlab. All chemicals and solvents were reagent grade and used without further purification. Where indicated, solvents were dried over activated powdered molecular sieves.

Preparation of Ligands $\mathbf{1}_n$, $\mathbf{2}_n$, $\mathbf{3}_8$. All the ligands were prepared in similar fashion. A general description is given here. Isonicotinic acid (8 g, 0.045 mol) was refluxed with a large excess of $SOCl_2$ for approximately 2−4 h until a clear solution was obtained. Excess thionyl chloride was removed in vacuo, leaving the acid chloride hydrochloride as a yellowish solid. Dry pyridine (50 mL) was added to give a yellow suspension. A stoichiometric amount of the appropriate amine (in the case of $\mathbf{1}_n$ or $\mathbf{3}_8$) or alcohol (in the case of $\mathbf{2}_n$) was added to the suspension, and the mixture stirred for 4 h, with heating as needed to facilitate stirring. The reaction was then poured into water, and $NaHCO_3$ was added until the pH was alkaline. The aqueous mixture was then extracted 3× with 100 mL of diethyl ether, and the organic layers were combined and washed twice with 100 mL of H_2O. The solvents were removed in vacuo. Purification of the various ligands was accomplished as described below. Purified yields varied from 60 to 86%.

For $\mathbf{1}_n$ the products were obtained as solids and recrystallized from diethyl ether. ^{1}H NMR: δ 8.69 (d, 2H, pyridine ring), 7.57 (d, 2H, pyridine ring), 6.34 (b, 1H, N*H*), 3.42 (dt, 2H, NH−CH_2−), 1.56 (tt, 2H, NH−CH$_2$−CH_2−), 1.15−1.30 (m, xH, NH−CH$_2$−CH$_2$−(CH_2)$_x$−CH$_3$), 0.84 (t, 3H, −CH_3).

For $\mathbf{2}_n$ where $n \geq 12$, the products were obtained as solids and recrystallized from diethyl ether; for $n < 12$, the products were obtained as oils and were purified by running through a silica gel column using 4:1 petroleum ether:tetrahydrofuran. ^{1}H NMR: δ 8.75 (2H, pyridine ring), 7.81 (2H, pyridine ring), 4.32 (t, 2H, COO−CH_2−), 1.73 (tt, 2H, COO−CH$_2$−CH_2−), 1.1−1.3 (m, xH, COO−CH$_2$−CH$_2$−(CH_2)$_x$−CH$_3$), 0.85 (t, 3H, −CH_3).

For $\mathbf{3}_8$, the solid obtained was purified by chromatography on silica gel using ethyl acetate. ^{1}H NMR: δ 8.68 (d, 2H, pyridine ring), 7.27 (d, 2H, pyridine ring), 3.53 and 3.16 (two triplets, 1H each, −NMe−CH_2), 3.08 and 2.90 (two singlets, 1.5H each, N−*Me*), 1.64 and 1.53 (two tt, 2H each, NMe−CH$_2$−CH_2−), 1.20−1.35 (m, xH, NMe−CH$_2$−CH$_2$−(CH_2)$_x$−CH$_3$), 0.84 (t, 3H, −CH_3).

Preparation of $Cu(\mathbf{1}_n)_2X_2$ or $Cu(\mathbf{3}_8)_2X_2$. CuX_2 (1.57 mmol) was dissolved in approximately 25−35 mL warm EtOH/H_2O (98:2). Two equivalents of the appropriate ligand were dissolved in a minimum amount of EtOH (with heating, if necessary) and added to the copper solution. The reaction was allowed to cool and the solid precipitate was filtered and washed with warm ethanol.

Preparation of $Cu(\mathbf{2}_n)_2X_2$. The preparation of these materials was identical to those above, except that when carried out in EtOH, the product typically contained varying amounts of a brown impurity, whose identity was not determined. It was found, however, that the same complexes could be prepared in acetone to give analytically pure materials, with no trace of the brown impurity.

Acknowledgment. This work was supported by ACS-PRF #32141-B1 and by Williams College Bronfman Shared Overhead Funds. The authors are most grateful to Professor Coleen Pugh at the University of Michigan and Professor Tim Swager and Scott Trzaska at MIT for all their assistance and the very generous use of their laboratory space and equipment.

CM970799M